

Complex phase diagram of $\text{Ba}_{1-x}\text{Na}_x\text{Fe}_2\text{As}_2$: A multitude of phases striving for the electronic entropy

L. Wang,^{*} F. Hardy, A. E. Böhmer,[†] T. Wolf, P. Schweiss, and C. Meingast[‡]*Institut für Festkörperphysik, Karlsruhe Institute of Technology, 76021 Karlsruhe, Germany*

(Received 9 October 2015; revised manuscript received 7 December 2015; published 19 January 2016)

The low-temperature electronic phase diagram of $\text{Ba}_{1-x}\text{Na}_x\text{Fe}_2\text{As}_2$, obtained using high-resolution thermal-expansion and specific-heat measurements, is shown to be considerably more complex than previously reported, containing nine different phases. Besides the magnetic C_2 and reentrant C_4 phases, we find evidence for an additional, presumably magnetic, phase below the usual spin-density-wave transition, as well as a possible incommensurate magnetic phase. All these phases coexist and compete with superconductivity, which is particularly strongly suppressed by the C_4 -magnetic phase due to a strong reduction of the electronic entropy available for pairing in this phase.

DOI: [10.1103/PhysRevB.93.014514](https://doi.org/10.1103/PhysRevB.93.014514)

High-temperature superconductivity in Fe-based systems usually emerges when a stripe-type antiferromagnetic spin-density wave (SDW) is suppressed by either doping or pressure [1–3]. The SDW transition is accompanied, or sometimes even slightly preceded, by a structural phase transition from a high-temperature tetragonal (C_4) to a low-temperature orthorhombic (C_2) state, which has sparked the lively debate about electronic nematicity and the respective role of spin and orbital physics in these materials [4–8]. In the hole-doped compounds, $\text{Ba}_{1-x}\text{Na}_x\text{Fe}_2\text{As}_2$, $\text{Ba}_{1-x}\text{K}_x\text{Fe}_2\text{As}_2$, and $\text{Sr}_{1-x}\text{Na}_x\text{Fe}_2\text{As}_2$, recent studies have shown that the C_4 symmetry is restored in a small pocket within the magnetic C_2 phase region [9–13]. Mössbauer studies on $\text{Sr}_{0.63}\text{Na}_{0.37}\text{Fe}_2\text{As}_2$ find that only half of the Fe sites carry a magnetic moment in this phase [12], which is consistent with the double- Q magnetic structure predicted within the itinerant spin-nematic scenario [6,9,12,14]. Moreover, neutron studies have shown that the spins flip from in-plane in the C_2 phase to out-of-plane in the C_4 reentrant phase [15], indicating that spin-orbit interactions cannot be neglected. In the $\text{Ba}_{1-x}\text{K}_x\text{Fe}_2\text{As}_2$ system, the reentrant C_4 phase reverts back to the C_2 phase near the onset of superconductivity, due to a stronger competition of the C_4 phase with superconductivity [10]. The presence of this phase in the hole-doped systems presents strong evidence that the physics of these Fe-based systems can be treated in an itinerant picture, and recent theoretical studies based upon the spin-nematic scenario can reproduce phase diagrams very similar to the experimental ones [16], as well as the spin reorientation in the C_4 phase if spin-orbit interactions are included [17].

Here, we reinvestigate in greater detail the low-temperature electronic phase diagram of $\text{Ba}_{1-x}\text{Na}_x\text{Fe}_2\text{As}_2$ using high-resolution thermal-expansion and specific-heat measurements, and show that it is considerably more complex than previously reported, containing nine different phases. Besides the usual C_2 and reentrant C_4 magnetic phases, we find evidence for an additional, presumably magnetic, C_2 phase, in which the

orthorhombic distortion is substantially reduced but still finite. These phases coexist and compete with superconductivity, which is particularly strongly suppressed by the reentrant C_4 phase. Further, we provide indications that the SDW transition becomes incommensurate above $x = 0.22$, which appears linked to the emergence of the C_4 phase at this composition. The surprising occurrence of this multitude of phases near the onset of superconductivity suggests a highly degenerate free-energy landscape near optimal doping, which may be related to the occurrence of superconductivity in the Fe-based systems.

Single crystals of $\text{Ba}_{1-x}\text{Na}_x\text{Fe}_2\text{As}_2$ were grown in alumina crucibles using a self-flux method with (Ba,Na): FeAs ratios 1:4–1:5. The crucibles were sealed in iron cylinders filled with argon gas. After heating to 1150–1170 °C, the furnace was cooled down slowly at rates between 0.3 and 0.5 °C/h to minimize the amount of flux inclusions. Near 940–1020 °C the furnace was turned upside down to separate the remaining liquid flux from the grown crystals and then cooled down to room temperature with intermediate holds to *in situ* anneal the crystals. Thermal expansion was measured using a high-resolution home-made capacitance dilatometer [18], which is several orders of magnitude more sensitive than traditional diffraction techniques. Heat capacity was measured using a Physical Property Measurement System from Quantum Design. The electronic specific heat was obtained by subtracting an appropriate phonon background [10,19,20]. Specifically, as demonstrated for $\text{Ba}_{1-x}\text{K}_x\text{Fe}_2\text{As}_2$ [10,21], the phonon background can be approximated as the weighted sum of the individual lattice contributions of its “constituents” [22], which are BaFe_2As_2 and NaFe_2As_2 for the present case. Since there are no crystals of NaFe_2As_2 , we determined the hypothetical NaFe_2As_2 phonon background by assuming that the electronic components at optimal doping of Na- and K-doped [10] systems are identical. This is quite reasonable, since both T_c and the heat capacity jumps at optimal doping are very similar in both systems. The Na content of seven single crystals [$x = 0.093(4), 0.182(2), 0.221(2), 0.283(2), 0.320(2), 0.360(3),$ and $0.401(4)$] used for the thermal-expansion and specific-heat measurements was accurately determined by four-circle single-crystal x-ray refinement of a small piece of the measured crystals. The Na content of the other crystals were interpolated between these fixed points using the SDW

^{*}liran.wang@kit.edu[†]Present address: The Ames Laboratory, U.S. Department of Energy, Iowa State University, Ames, Iowa 50011, USA.[‡]christoph.meingast@kit.edu

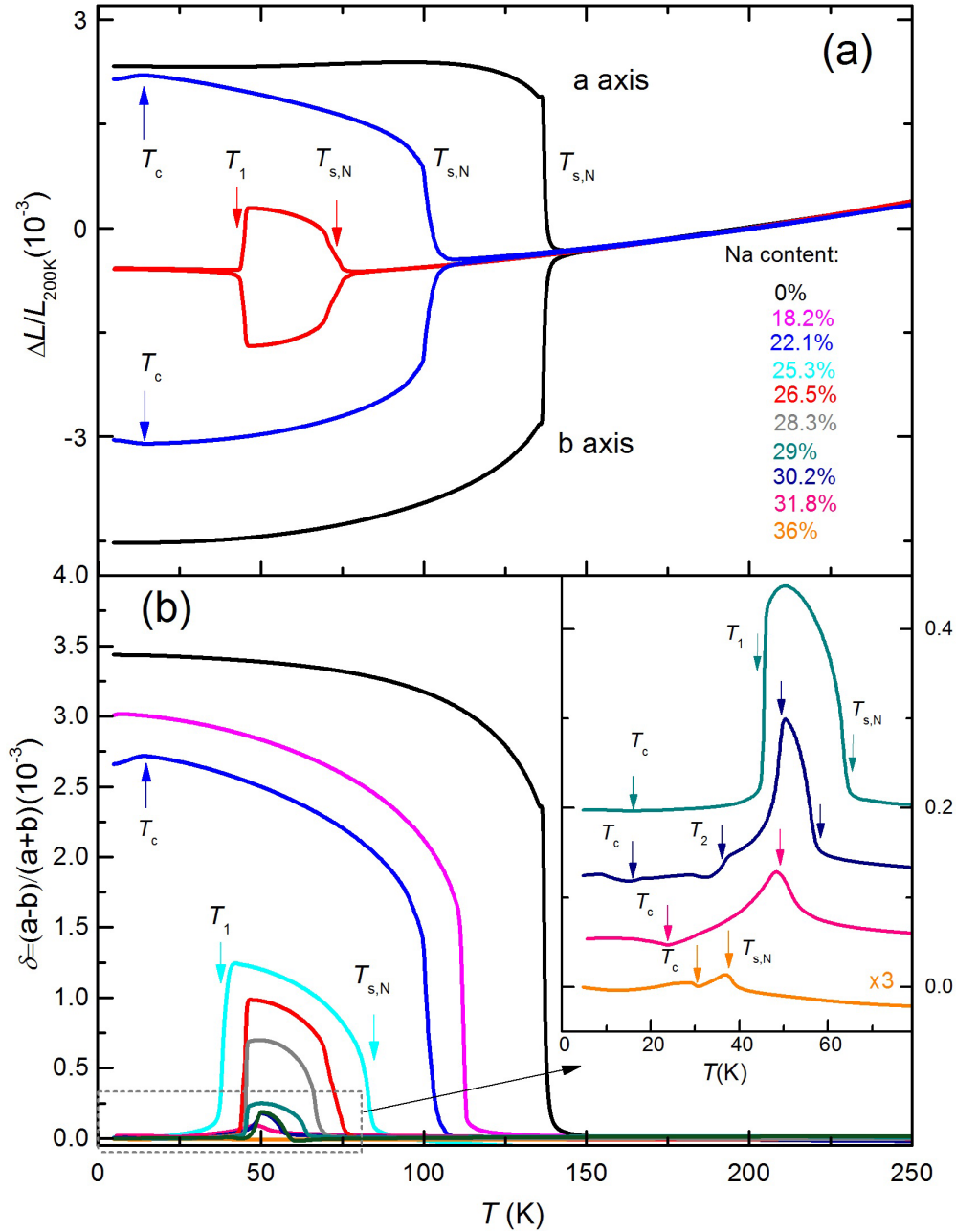


FIG. 1. (a) Relative length change, $\Delta L/L$, versus temperature of the orthorhombic lattice parameters a and b of $\text{Ba}_{1-x}\text{Na}_x\text{Fe}_2\text{As}_2$ for Na doping levels of $x = 0, 0.221, 0.265$ obtained using high-resolution capacitance dilatometry (see text for details). (b) Temperature dependence of the orthorhombic distortion $\delta = (a - b)/(a + b)$ inferred from the data in (a). The inset presents an expanded view of the data at higher doping levels. Vertical arrows indicate the location of the superconducting transition at T_c , the C_4 -reentrant transition at T_1 , and the stripe-type SDW transition at $T_{s,N}$.

transition temperature as a reference. The values of the structural parameters from our x-ray refinement are in good agreement with previous results [23].

Figure 1(a) presents the relative thermal expansion, $\Delta L/L$, measured along the a and b axes for three representative Na doping levels. As we have demonstrated previously [10,24], the shorter b axis in the low-temperature orthorhombic phase can be obtained directly by measuring the expansion of the crystal along the $[110]_T$ direction of the original tetragonal cell, because in this configuration the small force from the

dilatometer detwins the crystal. The larger a axis, on the other hand, is obtained by combining a “twinned” measurement (along $[100]_T$) with the “detwinned” data [10,24]. The expected orthorhombic splitting of the a and b lattice parameters at the SDW transition at $T_{s,N}$ is clearly observed for all three concentrations and reduces in magnitude with increasing Na content. For the $x = 0.265$ sample, this splitting suddenly disappears, within the accuracy of the measurements, at a first-order transition at $T_1 = 45$ K, which we identify with the C_4 magnetic phase [9,10].

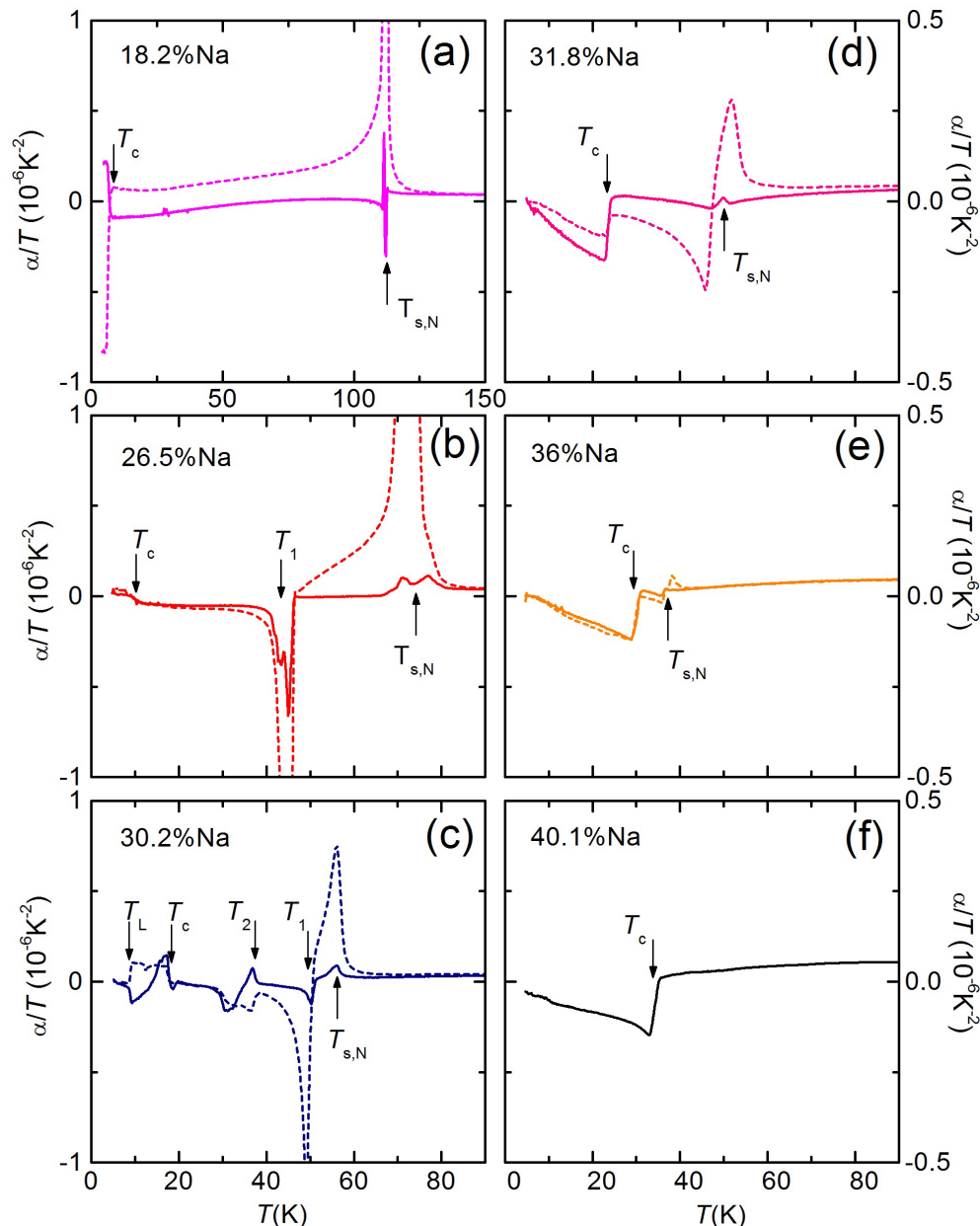


FIG. 2. (a)–(f) In-plane thermal expansion coefficients in “twinned” (solid lines) and “detwinned” (dashed lines) orientations versus T for Na concentrations of $x = 0.182, 0.265, 0.302, 0.318, 0.36,$ and 0.401 . The location of the various phase transitions is marked by vertical arrows. The breaking of the C_4 symmetry at $T_{s,N}$ in (a)–(e) is clearly indicated by the anisotropy of the “twinned” and “detwinned” expansion coefficients below $T_{s,N}$. On the other hand, the reentrant C_4 phase is characterized by equivalent expansion coefficients below T_1 in (b) and between T_2 and T_c in (c). The near optimally doped sample in (f) exhibits only a well-defined jump at T_c .

In order to study the doping evolution of these transitions in greater detail, we present in Fig. 1(b) the orthorhombic distortion, $\delta = (a - b)/(a + b)$, inferred from our thermal-expansion data for a number of compositions between $x = 0$ and $x = 0.36$. We detect clear signatures of the structural distortion associated with the SDW transition at $T_{s,N}$ all the way to $x = 0.36$, which is considerably higher than observed previously by neutron diffraction [9,23]. We note, however, that the orthorhombic splitting becomes extremely small in this high-doping region [see inset of Fig. 1(b)], which is probably why it was missed previously. The presence of the reentrant C_4 phase is signaled by a sudden disappearance of δ at T_1 ,

which we observe for $0.22 \leq x \leq 0.29$. The behavior of the lattice parameters changes dramatically for $x = 0.302$, where we observe a more gradual reduction of δ at T_1 , indicative of a second-order transition, followed by a previously unobserved transition at T_2 . Upon further doping, the transition at T_2 disappears and the transitions at $T_{s,N}$ and T_1 appear to merge together. The well-known reduction of δ at the superconducting transition in the C_2 SDW phase due to the competition between superconductivity and magnetism [24–26] is clearly observed for the crystal with $x = 0.221$, whereas the effect of superconductivity on the in-plane lattice parameters in the C_4 phase is too small to be seen in these curves.

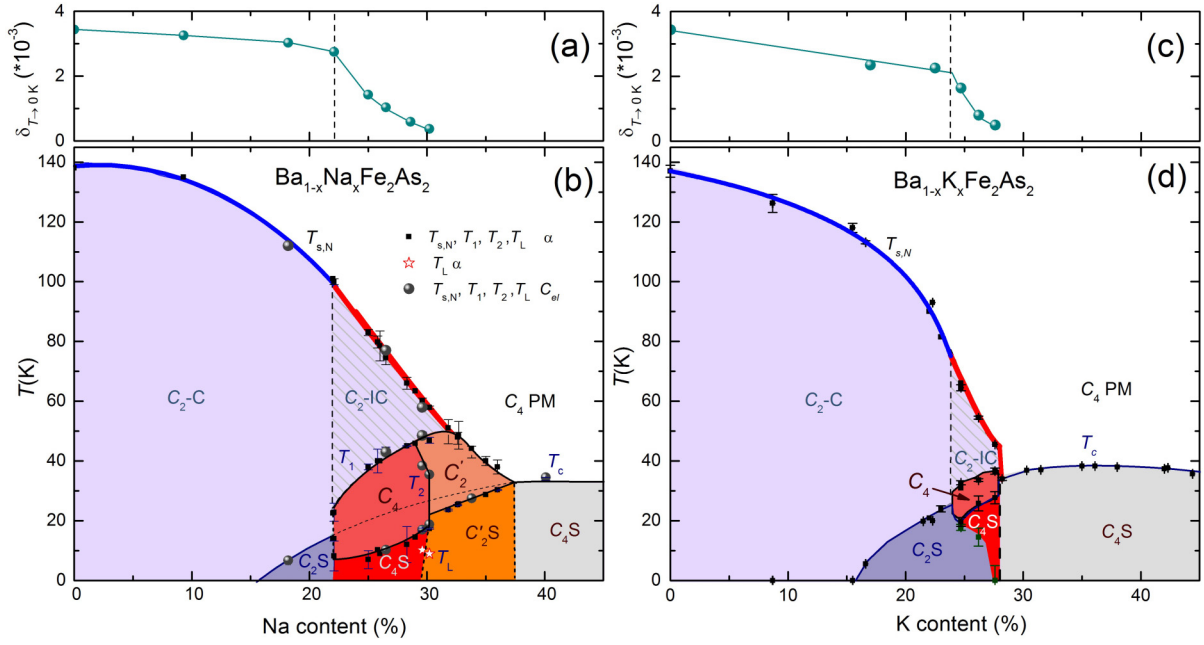


FIG. 3. Phase diagrams of Na- and K-doped systems. (a),(c) Extrapolated (to $T = 0$) orthorhombic distortion versus Na and K doping, respectively. (b) Electronic phase diagram of $Ba_{1-x}Na_xFe_2As_2$ obtained from thermal-expansion (squares) and specific-heat (circles) data revealing nine different phases (see text for details). (d) Phase diagram of $Ba_{1-x}K_xFe_2As_2$ from Ref. [10] for comparison. The kinks in (a) and (c), as well as the inflection points of $T_{s,N}$ in (b) and (d), near $x = 0.22-0.23$ are interpreted as marking a possible transition from a commensurate (C_2-C) phase to an incommensurate (C_2-IC) phase. This transition is indicated by the vertical dashed lines and the color transition of the $T_{s,N}$ line from blue to red. “S” stands for superconductivity.

The small anomalies associated with the onset of T_c , as well as the other phase transitions, are more clearly observed in the thermal-expansion coefficients, $\alpha(T) = \frac{1}{L} \frac{dL(T)}{dT}$, for the “twinned” and “detwinned” directions, which are presented as α/T versus T for representative Na contents in Fig. 2. Figure 2(a) displays data for the crystal with $x = 0.182$, which becomes orthorhombic below $T_{s,N} = 112$ K and superconducting below $T_c = 6.5$ K. The clear anisotropy of the in-plane expansion below $T_{s,N}$, as well as the anisotropic response at T_c , are indicative of the expected orthorhombic state at this doping level. We note that the small anisotropic tail above $T_{s,N}$ results from the small, but finite, uniaxial pressure we apply in our dilatometer [10]. In contrast to the behavior for $x = 0.182$, the anisotropy of the expansivity vanishes nearly completely below the transition at T_1 for the $x = 0.265$ sample [see Fig. 2(b)], indicating the reentrant tetragonal state below T_1 . As expected at the onset of superconductivity, small jumplike anomalies at T_c are observed for both directions. The behavior of the $x = 0.302$ crystal is more complicated [see Fig. 2(c)]. Here the crystal clearly becomes orthorhombic at $T_{s,N}$, then $\delta(T)$ decreases gradually between T_1 and T_2 [see inset of Fig. 1(b)], but remains orthorhombic. The expansivities for both orientations are equal below T_2 , suggesting that the system again enters a tetragonal state. The curves below T_c , however, again exhibit an anisotropic response, suggesting that the C_4 phase reverts back to the C_2' phase below T_c , in analogy to what has been observed in K-doped $BaFe_2As_2$ [10]. There is an additional sharp anomaly at $T_L = 10$ K for both orientations, which is, however, observed only upon heating, possibly indicating another phase transition with a large thermal hysteresis. Nearly identical behavior was observed in another crystal with

a similar composition. Our expansion data thus clearly show that the reentrant C_4 phase exists only in a limited temperature range between T_2 and T_c for $x = 0.302$. The transitions at T_2 and T_L both disappear for the next higher Na content [see Fig. 2(d)], and this sample also clearly displays strongly anisotropic thermal expansivities below $T_{s,N}$, which is incompatible with a C_4 symmetry. The $x = 0.36$ crystal [Fig. 2(e)] exhibits only very small effects at $T_{s,N}$ and T_1 . Finally, any signature of the anomaly at $T_{s,N}$ has disappeared in the crystal with $x = 0.401$, which only has a clear anomaly at $T_c = 35$ K.

The transition temperatures $T_{s,N}$, T_c , T_1 , T_2 , and T_L obtained by the thermal-expansion data shown in Figs. 1 and 2 allow us to construct a detailed phase diagram [see Fig. 3(b)]. Here, we have also included the transition temperatures extracted from the heat-capacity data (see Fig. 4). The phase diagram exhibits a remarkable degree of complexity, with a surprising number of additional (other than the usual C_2 -magnetic and superconductivity) phases emerging as magnetism is suppressed by Na doping. We note that these phases appear to emerge at the point where $T_{s,N}$ changes curvature from concave to convex near $x = 0.22$. This change is indicated by the changing color of the line from blue to red. The doping dependence of the extrapolated zero-temperature orthorhombic distortion of the C_2 phase [see Fig. 3(a)] illustrates this change even more clearly, with a very distinct kink near $x = 0.22$. We interpret the inflection point of $T_{s,N}(x)$ as a sign for a commensurate-to-incommensurate transition as expected in a simple mean-field SDW picture [27–29]. Previously, clear evidence for incommensurability has only been reported in electron doped $BaFe_2As_2$ [30–32]. Since we do not observe a splitting of the $T_{s,N}$ line into two transitions above

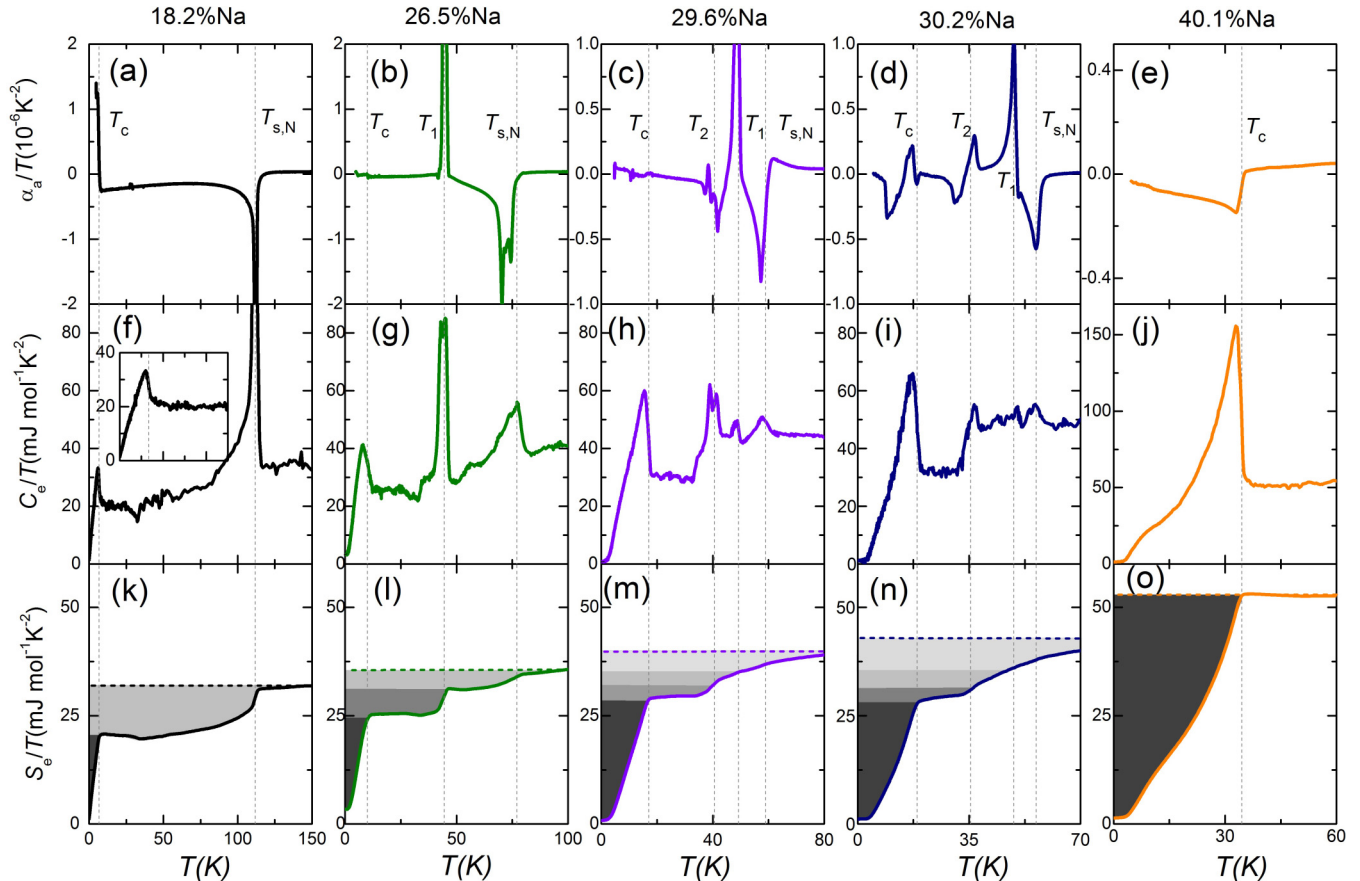


FIG. 4. (a)–(o) Temperature dependence of thermal expansion (α_a/T) [(a)–(e)], electronic heat capacity (C_e/T) [(f)–(j)], and electronic entropy (S_e/T) [(k)–(o)] for crystals with $x = 0.182, 0.265, 0.296, 0.302,$ and 0.401 . The different shades of gray represent the stepwise reduction of S_e/T from the high temperature paramagnetic phase to the low temperature superconducting state.

$x = 0.22$, we postulate the vertical dashed line to indicate the proposed commensurate-to-incommensurate transition. Such a vertical line implies a first-order transition, evidence of which is provided by the jumps of both T_1 and T_c at $x = 0.22$. In Figs. 3(c) and 3(d) we compare the present results to those of K-doped BaFe_2As_2 [10]. Similar to the Na-doped system, we also find an inflection point in its phase diagram [see Fig. 3(d)], as well as a kink in the $T = 0$ orthorhombic distortion [see Fig. 3(c)], at a K content at which the C_4 phase emerges [see Figs. 3(c) and 3(d)]. This strongly suggests that these are both common features in hole doped BaFe_2As_2 . In $\text{Ba}_{1-x}\text{Na}_x\text{Fe}_2\text{As}_2$ we observe, in addition to the magnetic C_4 phase, a previously unobserved phase [labeled C'_2 in Fig. 3(b)], which has a reduced, but finite, orthorhombic distortion. A similar phase is not observed in the K-doped system. Although we cannot examine the microscopic order in this phase using our macroscopic probes, the smooth doping variations of both $T_{s,N}$ and δ , suggest that this phase is probably also of magnetic origin, although some kind of charge [14] order cannot be excluded. Preliminary μSR measurements on a crystal with $x = 0.33$ provide evidence for a magnetic C'_2 phase [33]. Detailed investigations of the magnetic structure using, e.g., neutron scattering are highly desirable once large enough crystals become available.

In order to gain more insight into the different phases, we present the electronic heat capacity for several Na concentra-

tions in Fig. 4 together with thermal expansion of the a axis for comparison. As demonstrated in Figs. 3 and 4, the transition temperatures from the heat capacity (solid gray circles in Fig. 3) closely match those from the thermal expansion. With increasing Na doping, the steplike anomalies in C_e/T associated with superconductivity generally increase in size, whereas the anomalies associated with the magnetic transitions weaken, indicating the well-known competition between magnetism and superconductivity in the Fe-based systems [10,24–26]. This trend is made even more transparent in Figs. 4(k)–4(o), where we plot $S_e/T = (\int C_e/T dT)/T$, i.e., the electronic entropy divided by T , which for a Fermi liquid is expected to be constant. Upon entering the C_4 phase at 45 K for the $x = 0.265$ Na sample we observe a particularly large additional reduction of S_e/T at T_1 , which is more prominent than the anomaly at $T_{s,N}$, and apparently results in a large suppression of T_c and the condensation energy [equal to the black shaded area in Figs. 4(k)–4(o)] in the C_4 phase. This highlights the much stronger competition of superconductivity with the double- Q C_4 magnetic phase than with the usual magnetic C_2 phase, which was also observed in $\text{Ba}_{1-x}\text{K}_x\text{Fe}_2\text{As}_2$ [10]. However, in contrast to $\text{Ba}_{1-x}\text{K}_x\text{Fe}_2\text{As}_2$ [10], we find no evidence for a reemergence of the usual stripe-type C_2 phase below T_c . For the crystals with $x = 0.296$ and 0.302 , the largest (non superconducting) anomalies in C_e/T and S_e/T occur not at T_1 , but rather upon entering the C_4 phase at T_2 . Interestingly, the

S_e/T plot for both these samples [Figs. 4(m) and 4(n)] provide evidence for a pseudogap-like behavior above T_2 ; i.e., a gradual loss of density of states as the temperature is lowered. The competition of superconductivity with the C_2' phase appears to be much weaker than with the C_4 -magnetic phase, as evidenced by the increase of the superconducting condensation energy, as well as the rise of T_c seen in Fig. 3 within the C_2' phase. Finally, we note that the negligible residual C_e/T values of all of our samples (except for $x = 0.265$) demonstrate that our samples are of high quality and that doping away from the FeAs layer does not introduce pair breaking, as it does in Co-doped BaFe_2As_2 [34].

In summary, our detailed thermodynamic studies of $\text{Ba}_{1-x}\text{Na}_x\text{Fe}_2\text{As}_2$ show that the phase diagram of this system exhibits a surprising degree of complexity. As stripe-type magnetism is suppressed by Na-doping, two additional magnetic phases emerge, which coexist and compete with superconductivity. The emergence of these additional phases is shown

to be possibly triggered by a doping-induced commensurate-incommensurate transition near $x = 0.22$, which would provide further evidence for electronic itinerancy in these systems. There are many similarities between the phase diagrams of K- and Na-doped BaFe_2As_2 , and the differences are likely related to chemical pressure. Our previous studies on the K-doped system have shown that the phase boundaries are extremely pressure dependent [10], which has recently been confirmed by direct pressure experiments [35]. Importantly, the presently observed complexity of these phase diagram suggests a high degree of degeneracy of several energy scales as the optimally doped state is approached, which may also be related to the superconducting pairing mechanism.

We acknowledge fruitful discussions with Christian Bernhard, Markus Braden, Rafael Fernandes, Maria Gastiasoro, Benjamin Mallett, Jörg Schmalian, and Florian Waßer.

-
- [1] J. Paglione and R. L. Greene, *Nat. Phys.* **6**, 645 (2010).
 [2] D. C. Johnston, *Adv. Phys.* **59**, 803 (2010).
 [3] K. Ishida, Y. Nakai, and H. Hosono, *J. Phys. Soc. Jpn.* **78**, 062001 (2009).
 [4] H. Kontani, T. Saito, and S. Onari, *Phys. Rev. B* **84**, 024528 (2011).
 [5] R. M. Fernandes and J. Schmalian, *Supercond. Sci. Technol.* **25**, 084005 (2012).
 [6] R. M. Fernandes, A. V. Chubukov, and J. Schmalian, *Nat. Phys.* **10**, 97 (2014).
 [7] A. E. Böhmer, T. Arai, F. Hardy, T. Hattori, T. Iye, T. Wolf, H. v. Löhneysen, K. Ishida, and C. Meingast, *Phys. Rev. Lett.* **114**, 027001 (2015).
 [8] A. E. Böhmer and C. Meingast, *C. R. Phys.* **17**, 90 (2015).
 [9] S. Avcı, O. Chmaissem, J. Allred, S. Rosenkranz, I. Eremin, A. Chubukov, D. Bugaris, D. Chung, M. Kanatzidis, J.-P. Castellán, J. Schlueter, H. Claus, D. Khalyavin, P. Manuel, A. Daoud-Aladine, and R. Osborn, *Nat. Commun.* **5**, 3845 (2014).
 [10] A. E. Böhmer, F. Hardy, L. Wang, T. Wolf, P. Schweiss, and C. Meingast, *Nat. Commun.* **6**, 7911 (2015).
 [11] B. P. P. Mallett, P. Marsik, M. Yazdi-Rizi, T. Wolf, A. E. Böhmer, F. Hardy, C. Meingast, D. Munzar, and C. Bernhard, *Phys. Rev. Lett.* **115**, 027003 (2015).
 [12] J. M. Allred, K. M. Taddei, D. E. Bugaris, M. J. Krogstad, S. H. Lapidus, D. Y. Chung, H. Claus, M. G. Kanatzidis, D. E. Brown, J. Kang, R. M. Fernandes, I. Eremin, S. Rosenkranz, O. Chmaissem, and R. Osborn, *arXiv:1505.06175*.
 [13] E. Hassinger, G. Gredat, F. Valade, S. René de Cotret, A. Juneau-Fecteau, J.-Ph. Reid, H. Kim, M. A. Tanatar, R. Prozorov, B. Shen, H.-H. Wen, N. Doiron-Leyraud, and Louis Taillefer, *Phys. Rev. B* **86**, 140502(R) (2012).
 [14] M. N. Gastiasoro and B. M. Andersen, *Phys. Rev. B* **92**, 140506 (2015).
 [15] F. Waßer, A. Schneidewind, Y. Sidis, S. Wurmehl, S. Aswartham, B. Büchner, and M. Braden, *Phys. Rev. B* **91**, 060505 (2015).
 [16] J. Kang, X. Wang, A. V. Chubukov, and R. M. Fernandes, *Phys. Rev. B* **91**, 121104 (2015).
 [17] M. H. Christensen, J. Kang, B. M. Andersen, I. Eremin, and R. M. Fernandes, *Phys. Rev. B* **92**, 214509 (2015).
 [18] C. Meingast, B. Blank, H. Bürkle, B. Obst, T. Wolf, H. Wühl, V. Selvamanickam, and K. Salama, *Phys. Rev. B* **41**, 11299 (1990).
 [19] F. Hardy, T. Wolf, R. A. Fisher, R. Eder, P. Schweiss, P. Adelman, H. v. Löhneysen, and C. Meingast, *Phys. Rev. B* **81**, 060501 (2010).
 [20] F. Hardy, R. Eder, M. Jackson, D. Aoki, C. Paulsen, T. Wolf, P. Burger, A. Boehmer, P. Schweiss, P. Adelman, R. A. Fisher, and C. Meingast, *J. Phys. Soc. Jpn.* **83**, 014711 (2014).
 [21] F. Hardy (unpublished).
 [22] L. Y. Qiu and M. A. White, *J. Chem. Edu.* **78**, 1076 (2001).
 [23] S. Avcı, J. M. Allred, O. Chmaissem, D. Y. Chung, S. Rosenkranz, J. A. Schlueter, H. Claus, A. Daoud-Aladine, D. D. Khalyavin, P. Manuel, A. Llobet, M. R. Suhomel, M. G. Kanatzidis, and R. Osborn, *Phys. Rev. B* **88**, 094510 (2013).
 [24] A. E. Böhmer, P. Burger, F. Hardy, T. Wolf, P. Schweiss, R. Fromknecht, H. v. Löhneysen, C. Meingast, H. K. Mak, R. Lortz, S. Kasahara, T. Terashima, T. Shibauchi, and Y. Matsuda, *Phys. Rev. B* **86**, 094521 (2012).
 [25] S. Nandi, M. G. Kim, A. Kreyssig, R. M. Fernandes, D. K. Pratt, A. Thaler, N. Ni, S. L. Bud'ko, P. C. Canfield, J. Schmalian, R. J. McQueeney, and A. I. Goldman, *Phys. Rev. Lett.* **104**, 057006 (2010).
 [26] C. Meingast, F. Hardy, R. Heid, P. Adelman, A. Böhmer, P. Burger, D. Ernst, R. Fromknecht, P. Schweiss, and T. Wolf, *Phys. Rev. Lett.* **108**, 177004 (2012).
 [27] A. B. Vorontsov, M. G. Vavilov, and A. V. Chubukov, *Phys. Rev. B* **81**, 174538 (2010).
 [28] T. M. Rice, *Phys. Rev. B* **2**, 3619 (1970).
 [29] N. I. Kulikov and V. V. Tugushev, *Sov. Phys. Usp.* **27**, 954 (1984).
 [30] D. K. Pratt, M. G. Kim, A. Kreyssig, Y. B. Lee, G. S. Tucker, A. Thaler, W. Tian, J. L. Zarestky, S. L. Bud'ko, P. C. Canfield, B. N. Harmon, A. I. Goldman, and R. J. McQueeney, *Phys. Rev. Lett.* **106**, 257001 (2011).
 [31] P. Bonville, F. Rullier-Albenque, D. Colson, and A. Forget, *Europhys. Lett.* **89**, 67008 (2010).

- [32] H. Luo, R. Zhang, M. Laver, Z. Yamani, M. Wang, X. Lu, M. Wang, Y. Chen, S. Li, S. Chang, J. W. Lynn, and P. Dai, *Phys. Rev. Lett.* **108**, 247002 (2012).
- [33] B. Mallet and C. Bernhard (unpublished).
- [34] F. Hardy, P. Burger, T. Wolf, R. A. Fisher, P. Schweiss, P. Adelman, R. Heid, R. Fromknecht, R. Eder, D. Ernst, H. v. Löhneysen, and C. Meingast, *Europhys. Lett.* **91**, 47008 (2010).
- [35] E. Hassinger, G. Gredat, F. Valade, S. Rene de Cotret, O. Cyr-Choiniere, A. Juneau-Fecteau, J.-Ph. Reid, H. Kim, M. A. Tanatar, R. Prozorov, B. Shen, H.-H. Wen, N. Doiron-Leyraud, and Louis Taillefer, [arXiv:1512.05912](https://arxiv.org/abs/1512.05912).